



Article

Synthesis of an $\text{Ag}_3\text{PO}_4/\text{Nb}_2\text{O}_5$ Photocatalyst for the Degradation of Dye

Nur Syazwani Osman ¹, Siti Norhasimah Sulaiman ¹, Ernee Noryana Muhamad ¹, Hayati Mukhair ² , Sin Tee Tan ³ and Abdul Halim Abdullah ^{1,2,*} 

¹ Department of Chemistry, Faculty Science, Universiti Putra Malaysia, Serdang 43400, Malaysia; nur_syazwani611@yahoo.com (N.S.O.); sitinorhasimahsulaiman@gmail.com (S.N.S.); ernee@upm.edu.my (E.N.M.)

² Materials Synthesis and Characterization Laboratory, Institute of Advanced Technology, Serdang 43400, Malaysia; hayatimukhair@gmail.com

³ Department of Physics, Faculty Science, Universiti Putra Malaysia, Serdang 43400, Malaysia; tansintee@upm.edu.my

* Correspondence: halim@upm.edu.my

Abstract: In this work, the photocatalytic performance of Ag_3PO_4 , Nb_2O_5 and $\text{Ag}_3\text{PO}_4/\text{Nb}_2\text{O}_5$ hybrid photocatalysts to degrade methyl orange dye, MO, in an aqueous solution under visible light irradiation was evaluated. The Ag_3PO_4 and $\text{Ag}_3\text{PO}_4/\text{Nb}_2\text{O}_5$ photocatalysts, with various Ag to Nb molar ratios, were prepared using a facile precipitation method. The photocatalysts were characterized by X-ray diffraction, UV-Visible, X-ray Photoelectron, and Photoluminescence spectroscopies. Upon the addition of Ag_3PO_4 , the band gap energy of Nb_2O_5 decreased from 3.0 eV to 2.7 eV, indicating the possible use of the $\text{Ag}_3\text{PO}_4/\text{Nb}_2\text{O}_5$ hybrid photocatalysts under visible light irradiation. All of the prepared $\text{Ag}_3\text{PO}_4/\text{Nb}_2\text{O}_5$ catalysts exhibited higher photocatalytic performance than Ag_3PO_4 in degrading methyl orange dye under 23-watt visible light irradiation. The $\text{Ag}_3\text{PO}_4/\text{Nb}_2\text{O}_5$ catalyst, with a mole ratio of 2:1, exhibited the fastest MO degradation rate of $7.3 \times 10^{-2} \text{ min}^{-1}$, which is twice faster than that of Ag_3PO_4 . The catalyst also shows better stability, as it is reusable for up to six experimental cycles while maintaining its photocatalytic activity above 60%.

Keywords: $\text{Ag}_3\text{PO}_4/\text{Nb}_2\text{O}_5$; methyl orange; photocatalyst; photocatalytic activity; visible light



Citation: Osman, N.S.; Sulaiman, S.N.; Muhamad, E.N.; Mukhair, H.; Tan, S.T.; Abdullah, A.H. Synthesis of an $\text{Ag}_3\text{PO}_4/\text{Nb}_2\text{O}_5$ Photocatalyst for the Degradation of Dye. *Catalysts* **2021**, *11*, 458. <https://doi.org/10.3390/catal11040458>

Academic Editors: Vincenzo Vaiano and Olga Sacco

Received: 16 February 2021

Accepted: 26 March 2021

Published: 1 April 2021

Publisher's Note: MDPI stays neutral with regard to jurisdictional claims in published maps and institutional affiliations.



Copyright: © 2021 by the authors. Licensee MDPI, Basel, Switzerland. This article is an open access article distributed under the terms and conditions of the Creative Commons Attribution (CC BY) license (<https://creativecommons.org/licenses/by/4.0/>).

1. Introduction

Dyes, widely used in the textile, paint, ink, and paper industries, are the most significant chemical contaminants that cause water pollution [1]. Up to 200,000 tons of dyes are lost to effluents in textile industries every year during dyeing and finishing operations. The release of colored water in the effluents causes hazards and environmental problems. Since its discovery by Fujishima and Honda in 1972, heterogeneous photocatalysis has been widely explored as a water decontamination method [1]. Through heterogeneous photocatalysis, the complete mineralization of parents and their intermediate compounds is possible at ambient operating temperatures and pressures, and at low operational costs [2]. Nowadays, visible-light-driven photocatalysis has gained research interest, with Ag_3PO_4 being reported as a promising photocatalyst for the photodegradation of the aqueous dye solution. Its ability to utilize visible light irradiation is due to its narrow band gap energy. Unfortunately, self-photo corrosion is a significant problem, which means that the stability of Ag_3PO_4 remains an issue [3]. One of the initiatives to enhance the photocatalytic activity and the stability of the Ag_3PO_4 photocatalyst is by coupling it with other semiconductors, such as TiO_2 [4–6], ZnO [7], and CeO_2 [8]. This coupling method decreased the recombination probability of the electron-hole pairs, and enhanced the photocatalytic efficiency.

Niobium (V) oxide, Nb_2O_5 , which has a band gap energy (3.4 eV), which is similar to TiO_2 , is one of the promising photocatalysts, as it exhibits excellent photocatalytic performance in the photodegradation of dyes [9]. Although Souza et al. (2016) reported similar catalytic activity between Nb_2O_5 and TiO_2 -P25 in the degradation of textile wastewater [10], Prado and his co-workers (2008) showed that Nb_2O_5 is a more stable photocatalyst as it successfully maintained its 85% catalytic activity in indigo carmine degradation after ten reaction cycles [11].

This work aimed to produce a stable visible-light-driven photocatalyst by coupling Ag_3PO_4 with Nb_2O_5 . There are very few works on $\text{Ag}_3\text{PO}_4/\text{Nb}_2\text{O}_5$ photocatalysts available in the literature [3]. To the best of our knowledge, using a fluorescence lamp (23 W) as a source of light irradiation to degrade a dye over $\text{Ag}_3\text{PO}_4/\text{Nb}_2\text{O}_5$ photocatalysts has not been reported. Previously, the degradation of rhodamine B over $\text{Ag}_3\text{PO}_4/\text{Nb}_2\text{O}_5$ under simulated sunlight irradiation (Xe, 600 W) was reported [3]. In this work, $\text{Ag}_3\text{PO}_4/\text{Nb}_2\text{O}_5$ photocatalysts were synthesized via the deposition–precipitation method, and their photocatalytic activity was evaluated by the photodegradation of methyl orange (MO) under fluorescent light (23 W) irradiation. The experiments were performed under various parameters in order to determine the best-suited conditions for the degradation of MO. The effect of scavengers and a reusability test were conducted in order to determine the active species responsible for the degradation, and to evaluate the stability of the catalysts, respectively

2. Results

2.1. Characteristics of the Photocatalysts

Figure 1 shows the XRD patterns of the Ag_3PO_4 , Nb_2O_5 , and $\text{Ag}_3\text{PO}_4/\text{Nb}_2\text{O}_5$ catalysts. All of the diffraction peaks of pure Ag_3PO_4 and Nb_2O_5 were in good agreement with those of the cubic phase of Ag_3PO_4 (JCPDS No. 010840510) and the orthorhombic phase of Nb_2O_5 (JCPDS No. 000271003), respectively. The XRD pattern of the $\text{Ag}_3\text{PO}_4/\text{Nb}_2\text{O}_5$ catalysts clearly shows peaks of Ag_3PO_4 and Nb_2O_5 , confirming the presence of these materials in their pristine form in the $\text{Ag}_3\text{PO}_4/\text{Nb}_2\text{O}_5$ composite. The peak intensity of Ag_3PO_4 also increased corresponding to the increase in the content of Ag_3PO_4 in the catalyst.

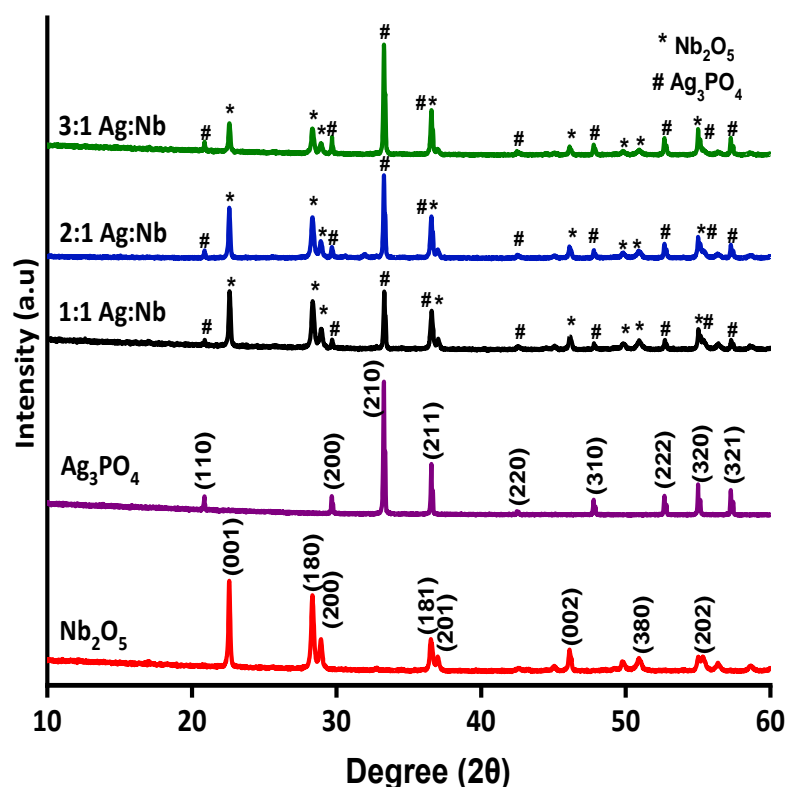


Figure 1. XRD patterns of the pure Nb_2O_5 , pure Ag_3PO_4 , and the prepared $\text{Ag}_3\text{PO}_4/\text{Nb}_2\text{O}_5$ photocatalysts.

The optical response of the catalysts in the visible light region was determined using the UV–Vis DRS spectrum. The data collected was transformed using the Kubelka-Munk function, and the band gap energy was extrapolated from the intercept of the x-axis of the Tauc plot (Figure 2). The band gap energy of Nb_2O_5 (3.3 eV) and Ag_3PO_4 (2.3 eV) is similar to the values reported in the literature [3,12]. Upon the addition of Ag_3PO_4 , the band gap energy of Nb_2O_5 slightly decreased to 3.2 eV.

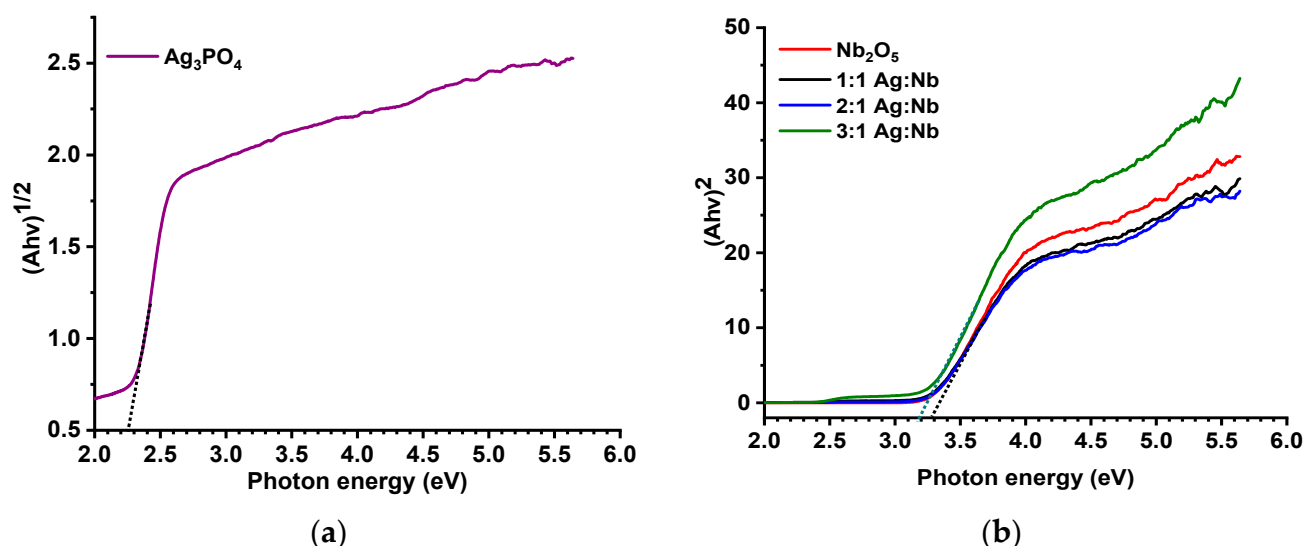


Figure 2. Plot of $(\alpha h\nu)^{1/2}$ against the eV of (a) pure Ag_3PO_4 , and (b) pure Nb_2O_5 , $\text{Ag:Nb} = 1:1$, $\text{Ag:Nb} = 2:1$, and $\text{Ag:Nb} = 3:1$ photocatalysts.

The optical properties and band structure of the samples were further evaluated using steady-state photoluminescence analysis. The results are presented in Figure 3. For the Nb_2O_5 , two broad peaks ranged from (i) the UV region: 350 nm to 400 nm, and (ii) the visible region: 400 nm to 550 nm. From Figure 3b, the first deconvoluted peak (blue) can be ascribed to the near band edge emission of the bulk Nb_2O_5 samples, whereas the second peak (green) can be referred to as the defect-assisted band alignment transition [13]. The Ag_3PO_4 sample also showed a broad emission peak from 400 nm to 600 nm, which can be deconvoluted into four peaks via Gaussian function analysis. The peaks were located at the wavelength 425 nm (violet), 480 nm (blue), 525 (green), and 575 nm (green). This result is consistent with the literature, stating that the carrier recombination arose from the shallow defect between the $[\text{PO}_4]$ and highly distorted tetrahedral $[\text{AgO}_4]$ clusters [14]. Upon the incorporation of Ag_3PO_4 into the Nb_2O_5 at a 1:1 molar ratio, it was found that the PL emission at the visible region from 400 nm to 600 nm (shallow defect) was quenched. This phenomenon signifies that the carrier recombination becomes more dominant in the heterojunction structure than the direct band edge at UV region of Nb_2O_5 (blue region in Figure 3b). In order to further evaluate the peak quenching, a normalised peak with respect to the direct band edge of Nb_2O_5 (382 nm) was conducted for all of the $\text{Ag}_3\text{PO}_4/\text{Nb}_2\text{O}_5$ and Nb_2O_5 samples. The result is presented in Figure 3d. It can be observed that the further increases of the Ag content in Nb_2O_5 have proved to suppress the PL intensity further in the shallow defect states, as compared to the Ag_3PO_4 sample. None of the defect states were observed in the Nb_2O_5 semiconductor material. This observation may be attributed to the agglomeration of the Ag_3PO_4 cluster, which contributed to the bulk trapping states. It is also worth mentioning that the increased Ag concentration can alter the charged polarization between the distorted Ag cluster, and could eventually promote intrinsic and extrinsic defect trapping states in the electronic structure of the Nb_2O_5 semiconductor materials. The plausible charge transfer mechanism is illustrated in Figure 3e. For the Nb_2O_5 sample, a charge transfer only occurred between the valence band and the conduction

band of the semiconductor material. For the $\text{Ag}_3\text{PO}_4/\text{Nb}_2\text{O}_5$ sample, a charge carrier was photoexcited from the valance band to the conduction band of Nb_2O_5 under the simulated sunlight. The charge carrier was later transferred to the conduction band of Ag_3PO_4 before it further underwent the reduction process with the analyte during the photodegradation process. Therefore, it is believed that the $\text{Ag}_3\text{PO}_4/\text{Nb}_2\text{O}_5$ semiconductor materials served as better photocatalysts than Nb_2O_5 , owing to its two charge transfer pathways, which lower the direct carrier recombination in the Nb_2O_5 semiconductor.

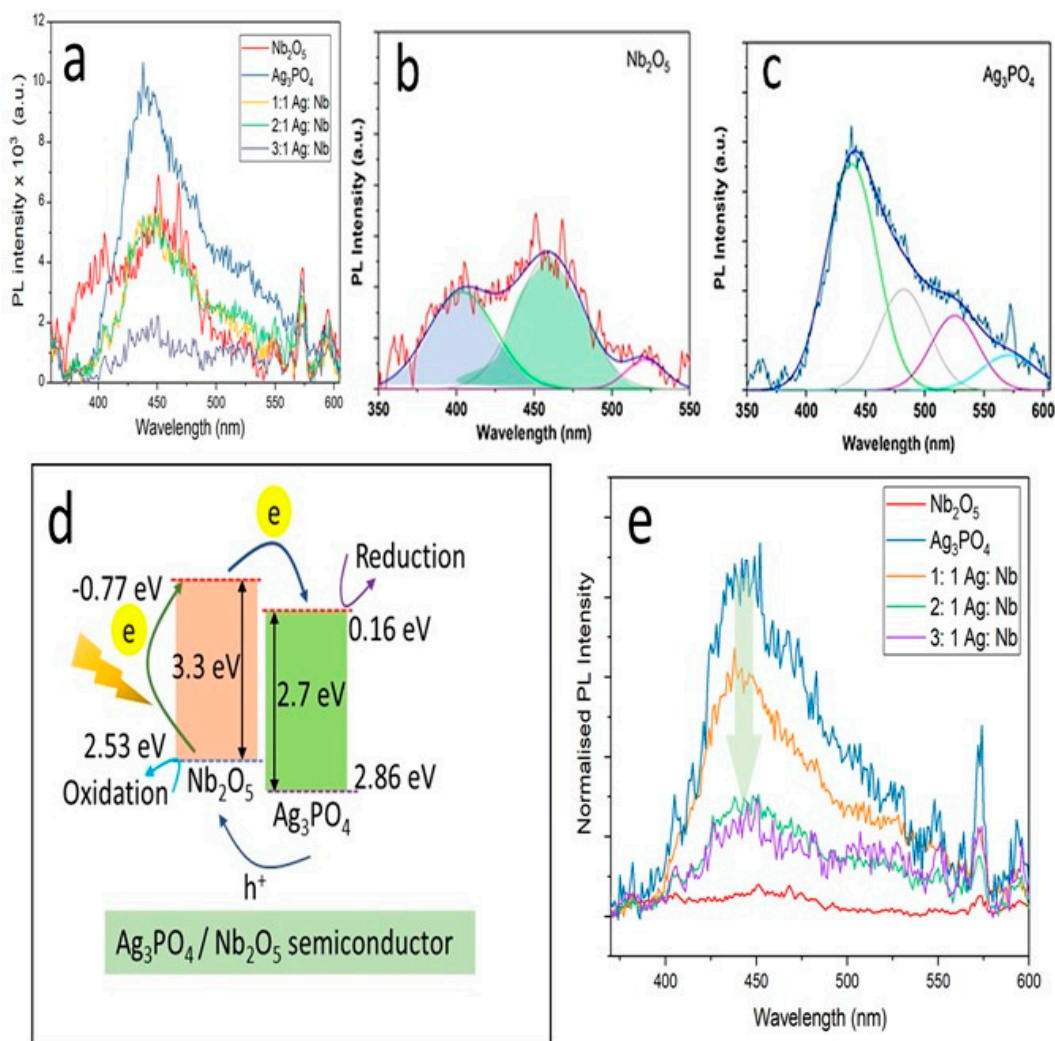


Figure 3. (a) Photoluminescence spectra of Nb_2O_5 , Ag_3PO_4 , and $\text{Ag}_3\text{PO}_4/\text{Nb}_2\text{O}_5$ nanocomposite with different molar ratios, and the deconvoluted sample for (b) Nb_2O_5 and (c) Ag_3PO_4 ; (d) the normalized peaks for all of the samples with respect to 382 nm of the direct band edge emission of Nb_2O_5 ; (e) the plausible charge transfer mechanism in Nb_2O_5 and $\text{Ag}_3\text{PO}_4/\text{Nb}_2\text{O}_5$ semiconductor materials.

The XPS spectrum of the 2:1 $\text{Ag}_3\text{PO}_4/\text{Nb}_2\text{O}_5$ photocatalyst (Figure 4)—which shows the presence of Ag, P, O, and Nb—verified the coexistence of Ag_3PO_4 and Nb_2O_5 in the composite. The peaks at 284.8 eV and 286.3 eV for C 1s belong to contaminant carbon C–C or C–O (Figure 4b). The peaks with the binding energy of 370.4 eV and 376.4 eV in the high-resolution XPS spectrum of Ag 3d (Figure 4c) are assigned to Ag 3d_{5/2} and Ag 3d_{3/2}, indicating the existence of Ag⁺ in the composite [15]. The peak of P 2p, observed at 132.6 eV (Figure 4d), is due to the P⁵⁺ of the phosphate. The deconvolution of the O 1s spectrum (Figure 4e) resulted in two peaks at 531.0 eV and 532.8 eV. The former corresponds to a crystal lattice oxygen of Ag_3PO_4 [16,17] and Nb_2O_5 [18,19]; the latter could be derived from the hydroxyl group on the surface of the catalyst. The high resolution of Nb 3d (Figure 4f) peaked for

Nb 3d_{5/2} at 207.3 eV, and Nb 3d_{3/2} at 210.0 eV corresponds to Nb⁵⁺, in good agreement with the binding energy of Nb₂O₅ [20].

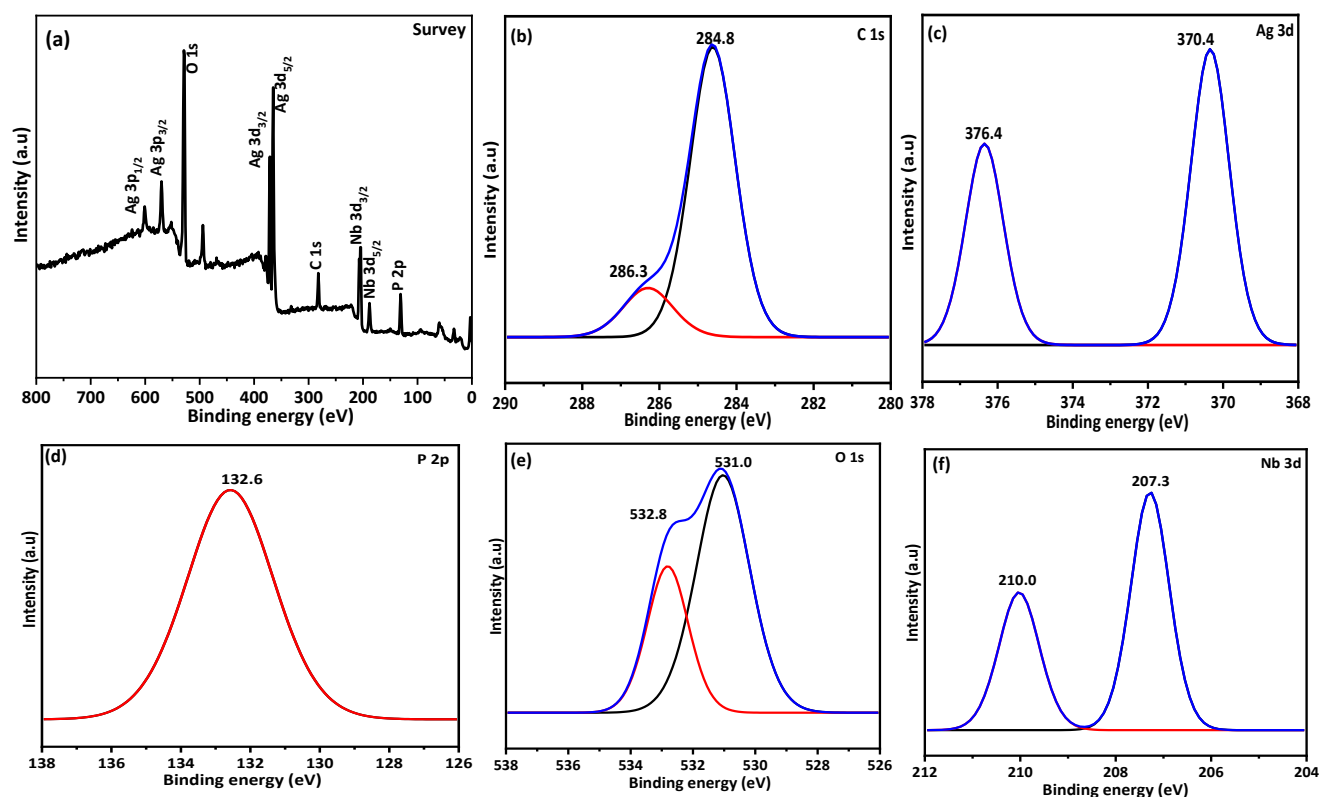


Figure 4. (a) XPS survey spectrum and high resolution spectra of (b) C 1s, (c) Ag 3d, (d) P 2p, (e) O 1s, and (f) Nb 3d of 2:1 Ag:Nb.

The morphology of Ag₃PO₄, Nb₂O₅, and Ag₃PO₄/Nb₂O₅ was illustrated in Figure 5. All of the samples exhibit similar morphology, being irregular spherical shapes. The image of Ag₃PO₄/Nb₂O₅ showed the severe agglomeration of the particles. EDX was employed in order to detect the elemental composition in the Ag₃PO₄/Nb₂O₅ composite photocatalyst, and the data are listed in Table 1. The as prepared catalyst different atomic percentage of Ag, Nb, P, and O. Based on the atomic percentage of Nb₂O₅ and Ag₃PO₄, the compositions of the catalysts were closely correlated with the mole ratio used in the preparation of the samples.

Table 1. The elemental composition of the Ag₃PO₄/Nb₂O₅ catalyst, as detected by EDX.

Sample	Elemental Composition (Atom %)				Ag:Nb
	3Ag	2Nb	P	O	
Ag:Nb (1:1)	13.37	7.83	4.14	74.66	4.4:4.0
Ag:Nb (2:1)	21.93	6.97	6.43	64.67	7.3:3.5
Ag:Nb (3:1)	30.18	6.73	8.86	54.23	10.1:3.3

The BET surface area and particle size determination of the Ag₃PO₄, Nb₂O₅, and Ag₃PO₄/Nb₂O₅ composite photocatalysts were analyzed by N₂ adsorption/desorption and Zetasizer; the data are summarized in Table 2. Based on the results, as the Ag₃PO₄ loading increased in the composites, a larger aggregate particle size was clearly observed compared to pristine Ag₃PO₄ and Nb₂O₅.

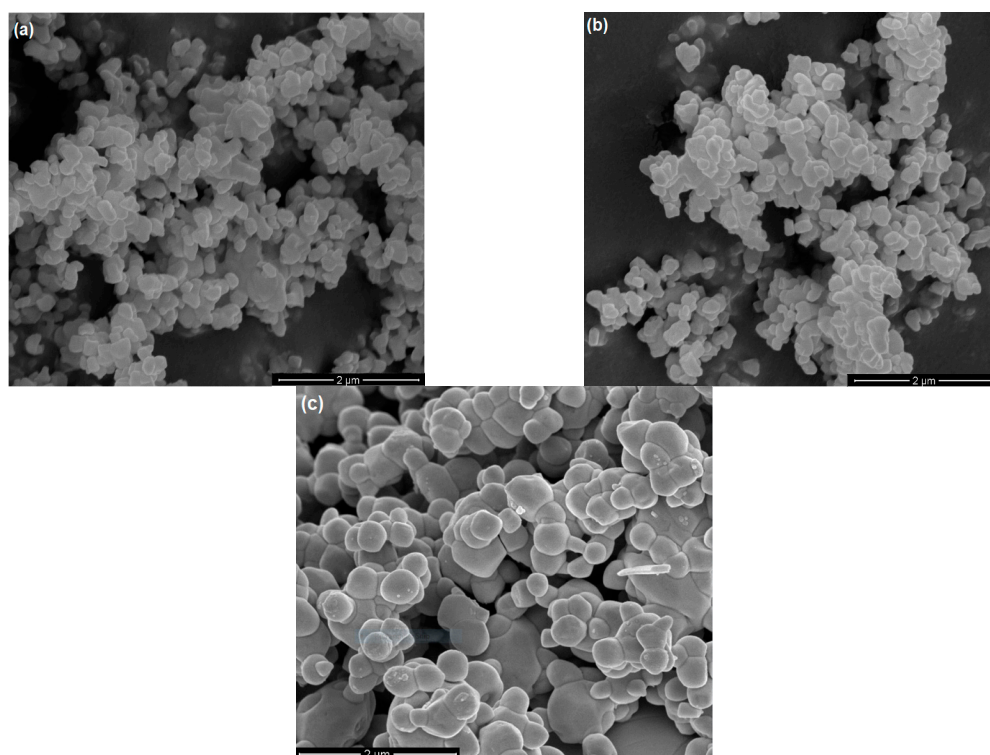


Figure 5. The morphology of the (a) Ag_3PO_4 , (b) Nb_2O_5 , and (c) $\text{Ag}_3\text{PO}_4/\text{Nb}_2\text{O}_5$ (Ag:Nb = 2:1).

Table 2. Particle size and BET surface area of the prepared catalysts.

Sample	Particle Size	BET Surface Area
	(μm)	(m^2g^{-1})
Ag_3PO_4	0.89 ± 0.11	1.63
Nb_2O_5	0.68 ± 0.06	6.92
Ag:Nb (1:1)	1.02 ± 0.11	1.70
Ag:Nb (2:1)	1.17 ± 0.09	0.89
Ag:Nb (3:1)	1.31 ± 0.12	1.07

The incorporation of Ag_3PO_4 into Nb_2O_5 resulted in the reduction of the surface area, which is attributed to the method of preparation. When contacted with the Nb_2O_5 , the Ag^+ ions would be adsorbed onto the Nb_2O_5 surface, possibly near the mouth of the pore or in the pore of Nb_2O_5 . When the phosphate solution was added into the solution mixture, Ag^+ would react to precipitate Ag_3PO_4 on the Nb_2O_5 . The formation of Ag_3PO_4 in the pore or on the mouth of the pore of Nb_2O_5 would block the pore, hence reducing the accessibility of the N_2 gas to the adsorption sites. Consequently, the prepared catalysts exhibited a lower surface area compared to pristine Nb_2O_5 and Ag_3PO_4 .

2.2. Photocatalytic Activity

The photocatalytic activity of the prepared photocatalysts was evaluated by the photodegradation of methyl orange, and the results are as shown in Figure 6. The degradation of MO by Nb_2O_5 was insignificant because it is inactive under visible light irradiation due to its wide band gap energy. The Ag_3PO_4 and $\text{Ag}_3\text{PO}_4/\text{Nb}_2\text{O}_5$ photocatalysts, however, exhibited a similar percentage of MO degradation, ranging from 91 to 96%. The experiment data was then fitted to the pseudo-first-order kinetic in order to determine the rate constant for the reaction. The MO degradation rate was faster when using $\text{Ag}_3\text{PO}_4/\text{Nb}_2\text{O}_5$ catalysts. The reaction rate initially increased with increasing Ag_3PO_4 loading up to a ratio of 2:1 before it decreased at a higher loading (3:1), which could be due to the agglomeration of

Ag_3PO_4 particles on the surface of the Nb_2O_5 . Because of its highest MO degradation rate (rate constant = 0.073 min^{-1}), the Ag:Nb = 2:1 was the suitable photocatalyst for this study.

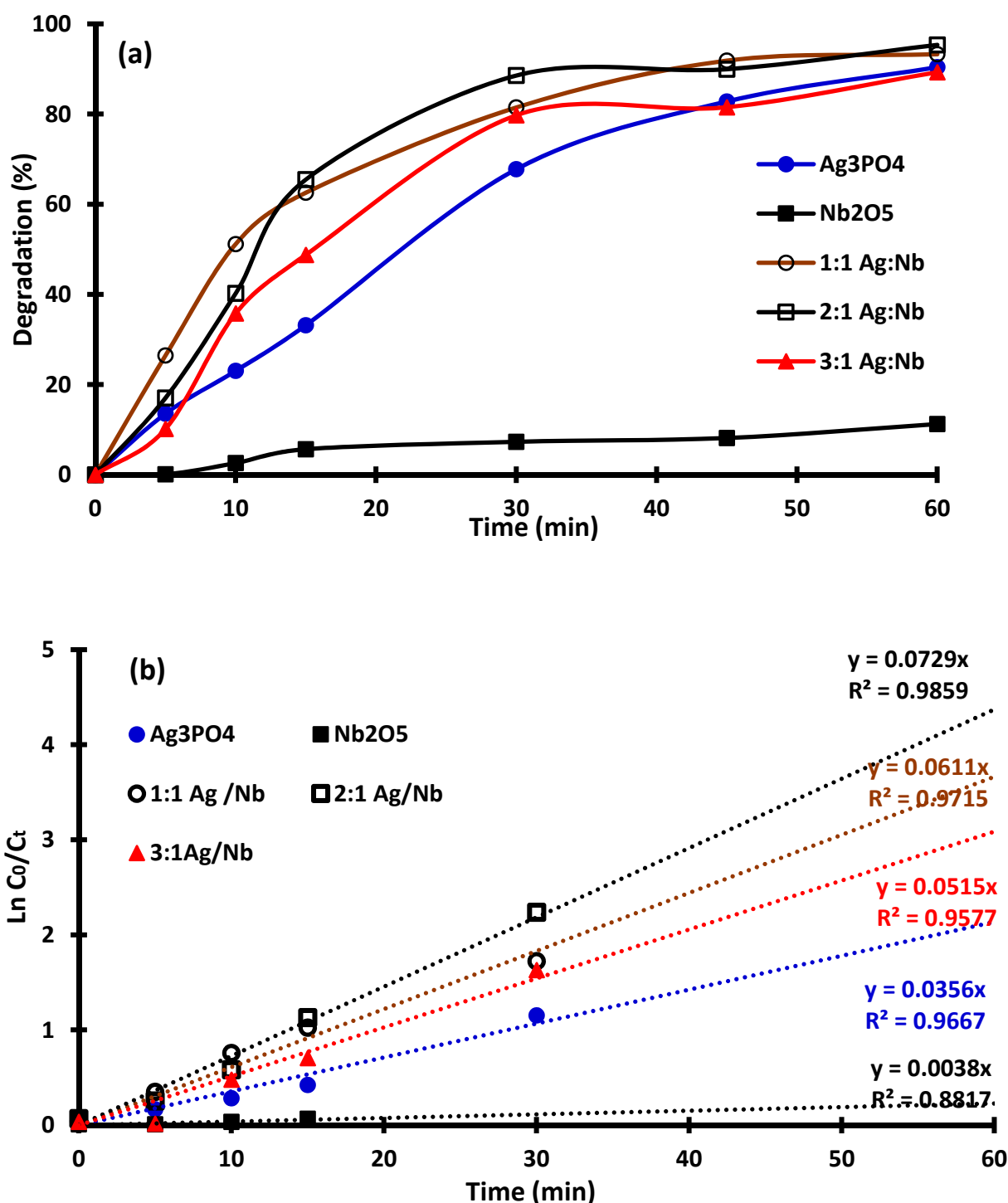


Figure 6. Plot of (a) the percentage degradation and (b) $\ln C_0/C_t$ against the irradiation time for the pure Ag_3PO_4 , pure Nb_2O_5 , and Ag:Nb = 1:1, Ag:Nb = 2:1 and Ag:Nb = 3:1 photocatalysts.

Several factors influence photocatalytic efficiency, including the mass of the photocatalyst and the concentration of the pollutant. Figure 7 shows the photodegradation activity using a various amount of Ag:Nb = 2:1 photocatalyst and the initial concentration of MO. The MO degradation rate increases with increasing catalyst mass, up to 0.5 g, before it

decreases at a higher catalyst mass (Figure 7a). The use of an excessive amount of catalyst loading reduces the degradation activity by increasing the light scattering effect and the opacity of the solution [21]. It also leads to the aggregation of the catalyst and reduces the interfacial area between the reaction solution and the photocatalyst. The fastest rate of degradation (Figure 7b) was observed when degrading 5 ppm of MO. The MO degradation rate, however, decreased with the increasing MO initial concentration. This decrement may occur due to the light screening effect, which reduces the photon's path length and the number of photons that arrive on the surface of the catalyst. Thus, it reduces the generation of electron-hole pairs, and consequently the photocatalytic activity of the photocatalyst [22].

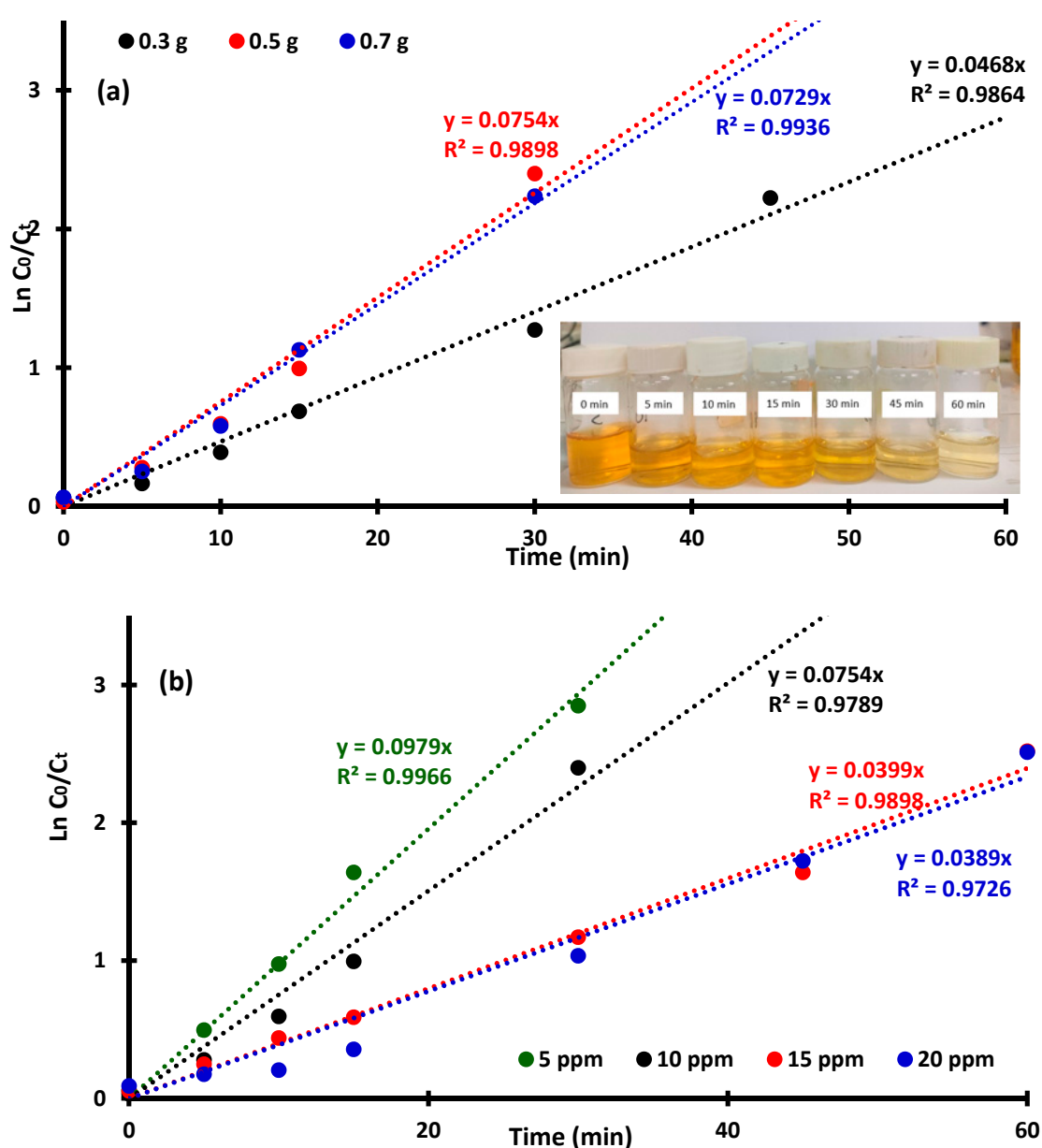


Figure 7. The rate of MO degradation at different (a) masses of catalyst (10 ppm MO) and (b) initial MO concentrations (0.5 g catalyst). The inset shows the progress of MO degradation (10 ppm) MO by 0.5 g Ag:Nb = 2:1 photocatalyst.

In order to determine the species responsible for the photodegradation, 10 mL of a scavenger solution—such as ethylene diamine tetraacetic acid (EDTA), tert-butanol, or benzoquinone (BQ)—was added to the MO solution. These solutions scavenge the h^+ ,

$\bullet\text{OH}$, and $\bullet\text{O}_2^-$ radicals, respectively. In the absence of the scavengers, the photocatalytic degradation of MO was 96% (Figure 8). Upon the addition of the EDTA and BQ solutions, the photodegradation decreased significantly to 1% and 32%, respectively. However, there was no significant effect on the photodegradation efficiency observed with the addition of tert-butanol. These results demonstrate that the h^+ and $\bullet\text{O}_2^-$ species are responsible for the photodegradation of MO.

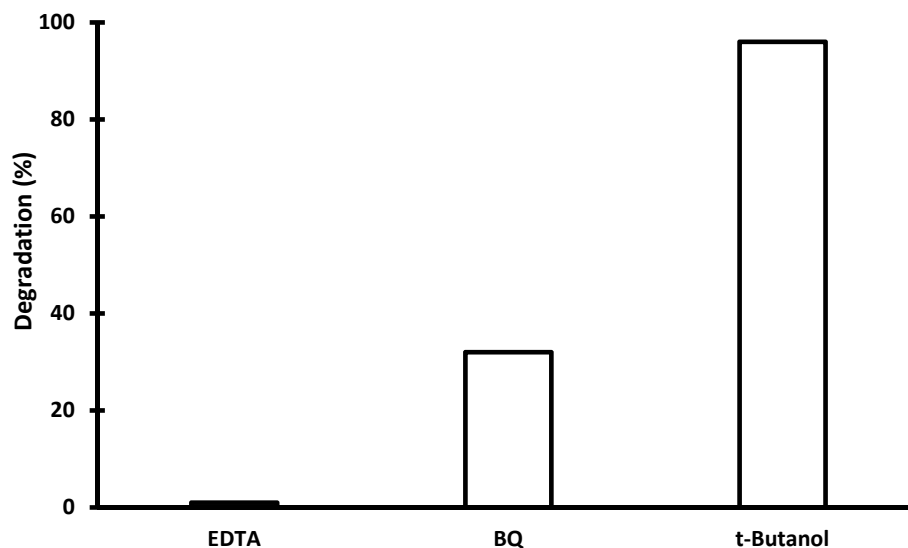


Figure 8. Comparison of the photocatalytic activities of the Ag:Nb = 2:1 photocatalyst with different scavengers during the photocatalytic reaction under 60 min visible light irradiation.

2.3. Reusability of the $\text{Ag}_3\text{PO}_4/\text{Nb}_2\text{O}_5$ Photocatalyst

The catalyst's lifetime is an essential parameter of the photocatalytic degradation process, so it is crucial to evaluate the catalyst's reusability for practical applications. As shown in Figure 9, the decrease in the photocatalytic efficiency of the Ag:Nb = 2:1 photocatalyst was gradual, but remained above 60% up to the fifth cycle of the photodegradation experiment. This gradual loss might be due to the self-photo corrosion of Ag_3PO_4 . The enhanced photocatalytic activity and stability of the Ag:Nb = 2:1 photocatalyst may be due to the insoluble Nb_2O_5 layer, which can effectively protect the dissolution of Ag_3PO_4 to Ag^+ ions, thus improving the structural stability of the photocatalyst.

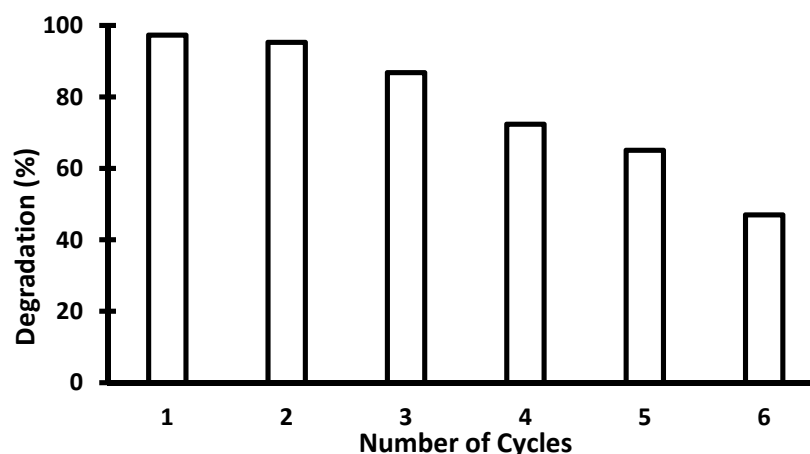


Figure 9. Reusability of the Ag:Nb = 2:1 photocatalyst in MO degradation.

3. Materials and Methods

3.1. The Synthesis of the $\text{Ag}_3\text{PO}_4/\text{Nb}_2\text{O}_5$ Photocatalyst

$\text{Ag}_3\text{PO}_4/\text{Nb}_2\text{O}_5$ photocatalysts with different Ag_3PO_4 to Nb_2O_5 mole ratios were prepared via a facile deposition–precipitation method. In a typical experiment, a fixed amount of Nb_2O_5 (Merck, Darmstadt, Germany) was dispersed in 150 mL deionized water and sonicated for 30 min. Various amounts of AgNO_3 salt (Merck, Germany) were added into the solution mixture and magnetically stirred for 30 min. In total, 150 mL of disodium hydrogen phosphate and Na_2HPO_4 (Fisher Scientific, Shah Alam, Malaysia) solution were added dropwise into the solution mixture with continuous stirring. The mole ratio of AgNO_3 to Na_2HPO_4 was kept constant at 3:1 in order to produce the Ag_3PO_4 catalyst. The yellow precipitate formed was collected by filtration, washed several times with distilled water and ethanol, and dried in an oven at 80 °C overnight. The final product was ground and characterized before being used in the photodegradation studies. A similar procedure, without the addition of Nb_2O_5 , was employed to produce a pure Ag_3PO_4 photocatalyst.

3.2. Characterization of the Catalyst

The crystalline phase of the catalysts was analyzed using an XRD 6000 (Shimadzu, Kyoto, Japan) with $\text{Cu-K}\alpha$ radiation, operated at $\lambda = 1.54$ nm, 30 kV, and 40 mA. The morphology and elemental composition of the catalysts were determined using a FESEM Nova Nanosem 230 (Fei, Eindhoven, The Netherlands) integrated with an energy dispersive X-ray detector. A fluorescence spectrophotometer (Perkin Elmer LS55, Waltham, MA, USA) with a wavelength excitation of 290 nm was used to record the photoluminescence spectra of the samples. The UV–vis diffuse reflectance spectra were recorded by a Shimadzu UV 3101 spectrophotometer at a wavelength between 220 and 800 nm. The chemical state of the elements was analysed using Auger Electron Spectroscopy with an X-Ray Photoelectron Spectrometer (Axis Ultra DLD, Kratos, Manchester, UK). The BET surface area was obtained by the application of BET modelling, conducting in TriStar II Plus (Micromeritics, Norcross, GA, USA). The particle size measurement was determined by Zetasizer, (Malvern Instruments, Worcestershire, UK).

3.3. Photoactivity of the $\text{Ag}_3\text{PO}_4/\text{Nb}_2\text{O}_5$ Photocatalyst

The photodegradation of methyl orange dye (MO) was performed in a glass photoreactor, as shown in Figure 10. A fixed amount of photocatalyst was added into 0.5 L of 10 ppm MO solution and stirred in the dark for 30 min. Air was bubbled into the solution throughout the experiment in order to ensure a constant supply of oxygen. During irradiation with a compact fluorescent lamp (23 W, Phillips, 1600 Lumens), an aliquot of the sample was withdrawn from the bulk solution at predetermined time intervals and filtered to remove catalyst particles. The samples were analyzed using UV–vis Perkin-Elmer Lambda 30 spectrophotometer at λ_{max} of 464.4 nm in order to determine the MO dye's residual concentration. The percentage of degradation and the amount of MO degraded are calculated using Equations (1) and (2), respectively:

$$\% \text{ Degradation} = \frac{C_0 - C_t}{C_0} \times 100\% \quad (1)$$

$$\text{Amount of degraded (mg/g)} = \frac{C_0 - C_t \left(\frac{\text{mg}}{\text{L}} \right)}{\text{mass of catalyst (g)}} \times V \text{ (L)} \quad (2)$$

where C_0 is the initial MO concentration, C_t is the MO concentration at a time 't', and V is the volume of the MO solution used in the reaction.

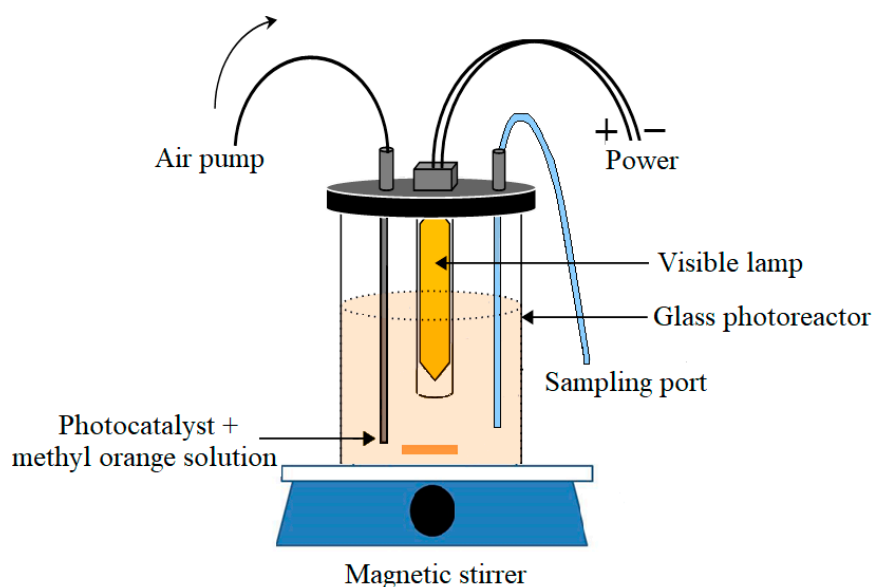


Figure 10. Schematic representation of the photocatalytic reactor for the photodegradation of methyl orange.

3.4. Reusability Test

The reusability of the catalyst was evaluated by performing several cycles of MO photodegradation in the the best-suited conditions. Once the first experiment ended, the treated MO solution was removed by decantation after the catalyst had settled at the bottom of the photoreactor. A fresh MO solution was then added to the reactor in order to start the next cycle.

4. Conclusions

The $\text{Ag}_3\text{PO}_4/\text{Nb}_2\text{O}_5$ photocatalysts, synthesized via the deposition–precipitation method, exhibited irregular and spherical shapes with a surface area of $0.89\text{--}1.70\text{ m}^2/\text{g}$. The catalysts also showed a faster MO degradation rate than Ag_3PO_4 . $\text{Ag}_3\text{PO}_4/\text{Nb}_2\text{O}_5$, and a molar ratio of 2:1 showed the highest photocatalytic degradation of 10 ppm MO (96%) with a catalyst loading of 0.5 g. The incorporation of Nb_2O_5 in Ag_3PO_4 enhanced the catalysts' photocatalytic performance and stability, and thus can be used effectively under visible light irradiation for up to five cycles. h^+ and $\bullet\text{O}_2^-$ are the main active species for the degradation.

Author Contributions: Conceptualization, A.H.A., N.S.O., and E.N.M.; methodology, A.H.A., N.S.O., S.T.T., and E.N.M.; validation, A.H.A., N.S.O., S.T.T. and H.M.; formal analysis, A.H.A., N.S.O., S.N.S., and H.M.; investigation, N.S.O., S.N.S., and H.M.; writing—original draft preparation, N.S.O., S.N.S., and H.M.; writing—review and editing, A.H.A., S.T.T., and E.N.M.; supervision, A.H.A. and E.N.M.; project administration, A.H.A.; funding acquisition, A.H.A., N.S.O., and E.N.M. All authors have read and agreed to the published version of the manuscript.

Funding: This research was funded by Universiti Putra Malaysia, grant number GPB-9629300.

Data Availability Statement: The data presented in this study are available on request from the corresponding author.

Acknowledgments: The authors would like to acknowledge Universiti Kebangsaan Malaysia and Universiti Teknologi MARA for the services and technical support provided for the research works.

Conflicts of Interest: The authors declare no conflict of interest.

References

- Mandal, S.; Natarajan, S.; Tamilselvi, A.; Mayadevi, S. Photocatalytic and antimicrobial activities of zinc ferrite nanoparticles synthesized through soft chemical route: A magnetically recyclable catalyst for water/wastewater treatment. *J. Environ. Chem. Eng.* **2016**, *4*, 2706–2712. [\[CrossRef\]](#)
- Chong, M.N.; Jin, B.; Chow, C.W.K.; Saint, C. Recent developments in photocatalytic water treatment technology: A review. *Water Res.* **2010**, *44*, 2997–3027. [\[CrossRef\]](#) [\[PubMed\]](#)
- Shao, R.; Zeng, X.; Cao, Z.; Dong, H.; Wang, L.; Wang, F.; Liu, J.; Li, Z.; Liang, Q. A novel $\text{Ag}_3\text{PO}_4/\text{Nb}_2\text{O}_5$ fiber composite with enhanced photocatalytic performance and stability. *RSC Adv.* **2015**, *5*, 102101–102107. [\[CrossRef\]](#)
- Cai, L.; Long, Q.; Yin, C. Synthesis and characterization of high photocatalytic activity and stable $\text{Ag}_3\text{PO}_4/\text{TiO}_2$ fibers for photocatalytic degradation of black liquor. *Appl. Surf. Sci.* **2014**, *319*, 60–67. [\[CrossRef\]](#)
- Zhao, F.M.; Pan, L.; Wang, S.; Deng, Q.; Zou, J.J.; Wang, L.; Zhang, X. $\text{Ag}_3\text{PO}_4/\text{TiO}_2$ composite for efficient photodegradation of organic pollutants under visible light. *Appl. Surf. Sci.* **2014**, *317*, 833–838. [\[CrossRef\]](#)
- Yao, W.; Zhang, B.; Huang, C.; Ma, C.; Song, X.; Xu, Q. Synthesis and characterization of high efficiency and stable $\text{Ag}_3\text{PO}_4/\text{TiO}_2$ visible light photocatalyst for the degradation of methylene blue and rhodamine B solutions. *J. Mater. Chem.* **2012**, *22*, 4050–4055. [\[CrossRef\]](#)
- Dong, C.; Wu, K.L.; Li, M.R.; Liu, L.; Wei, X.W. Synthesis of $\text{Ag}_3\text{PO}_4\text{-ZnO}$ nanorod composites with high visible-light photocatalytic activity. *Catal. Commun.* **2014**, *46*, 32–35. [\[CrossRef\]](#)
- Zhang, W.; Hu, C.; Zhai, W.; Wang, Z.; Sun, Y.; Chi, F.; Ran, S.; Liu, X.; Lv, Y. Novel $\text{Ag}_3\text{PO}_4/\text{CeO}_2$ p-n Hierarchical Heterojunction with Enhanced Photocatalytic Performance. *Mater. Res.* **2016**, *19*, 673–679. [\[CrossRef\]](#)
- Chen, J.; Wang, H.; Huang, G.; Zhang, Z.; Han, L.; Song, W.; Li, M.; Zhang, Y. Facile synthesis of urchin-like hierarchical Nb_2O_5 nanospheres with enhanced visible light photocatalytic activity. *J. Alloys Compd.* **2017**, *9*, 19–28. [\[CrossRef\]](#)
- Souza, R.P.; Freitas, T.K.F.S.; Domingues, F.S.; Pezoti, O.; Ambrosio, E.; Ferrari-Lima, A.M.; Garcia, J.C. Photocatalytic activity of TiO_2 , ZnO and Nb_2O_5 applied to degradation of textile wastewater. *J. Photochem. Photobiol. A Chem.* **2016**, *329*, 9–17. [\[CrossRef\]](#)
- Prado, A.G.S.; Bolzon, L.B.; Pedroso, C.P.; Moura, A.O.; Costa, L.L. Nb_2O_5 as efficient and recyclable photocatalyst for indigo carmine degradation. *Appl. Catal. B Environ.* **2008**, *82*, 219–224. [\[CrossRef\]](#)
- Morais, L.A.; Adán, C.; Araujo, A.S.; Guedes, A.P.M.A.; Marugán, J. Synthesis, Characterization, and Photonic Efficiency of Novel Photocatalytic Niobium Oxide Materials. *Glob. Chall.* **2017**, *1*, 1700066. [\[CrossRef\]](#)
- He, J.; Hu, Y.; Wang, Z.; Lu, W.; Yang, S.; Wu, G.; Wang, Y.; Wang, S.; Gu, H.; Wang, J. Hydrothermal growth and optical properties of Nb_2O_5 nanorod arrays. *J. Mater. Chem. C* **2014**, *2*, 8185–8190. [\[CrossRef\]](#)
- Botelho, G.; Andres, J.; Gracia, L.; Matos, L.S.; Longo, E. Photoluminescence and Photocatalytic Properties of Ag_3PO_4 Microcrystals: An Experimental and Theoretical Investigation. *ChemPlusChem* **2016**, *81*, 202–212. [\[CrossRef\]](#) [\[PubMed\]](#)
- Cui, X.; Zheng, Y.F.; Zhou, H.; Yin, H.Y.; Song, X.C. The effect of synthesis temperature on the morphologies and visible light photocatalytic performance of Ag_3PO_4 . *J. Taiwan Inst. Chem. Eng.* **2016**, *60*, 328–334. [\[CrossRef\]](#)
- Katsumata, H.; Sakai, T.; Suzuki, T.; Kaneco, S. Highly Efficient Photocatalytic Activity of $\text{g-C}_3\text{N}_4/\text{Ag}_3\text{PO}_4$ Hybrid Photocatalysts through Z-Scheme Photocatalytic Mechanism under Visible Light. *Ind. Eng. Chem. Res.* **2014**, *53*, 8018–8025. [\[CrossRef\]](#)
- Li, Y.; Yu, L.; Li, N.; Yan, W.; Li, X. Heterostructures of $\text{Ag}_3\text{PO}_4/\text{TiO}_2$ mesoporous spheres with highly efficient visible light photocatalytic activity. *J. Colloid Interface Sci.* **2015**, *450*, 246–253. [\[CrossRef\]](#)
- Qamar, M.; Abdalwadoud, M.; Ahmed, M.I.; Azad, A.M.; Merzougui, B.; Bukola, S.; Yamani, Z.H.; Siddiqui, M.N. Single-Pot Synthesis of 001-Faceted N-Doped Nb_2O_5 /Reduced Graphene Oxide Nanocomposite for Efficient Photoelectrochemical Water Splitting. *ACS Appl. Mater. Interfaces* **2015**, *7*, 17954–17962. [\[CrossRef\]](#) [\[PubMed\]](#)
- Xue, J.; Wang, R.; Zhang, Z.; Qiu, S. Facile preparation of C, N co-modified Nb_2O_5 nanoneedles with enhanced visible light photocatalytic activity. *Dalton Trans.* **2016**, *45*, 16519–16525. [\[CrossRef\]](#)
- Kong, L.; Zhang, C.; Wang, J.; Qiao, W.; Ling, L.; Long, D. Nanoarchitected Nb_2O_5 hollow, Nb_2O_5 @carbon and NbO_2 @carbon Core-Shell Microspheres for Ultrahigh-Rate Intercalation Pseudocapacitors. *Sci. Rep.* **2016**, *6*, 1–10. [\[CrossRef\]](#)
- Li, R.; Song, X.; Huang, Y.; Fang, Y.; Jia, M.; Ma, W. Visible-light photocatalytic degradation of azo dyes in water by Ag_3PO_4 : An unusual dependency between adsorption and the degradation rate on pH value. *J. Mol. Catal. A Chem.* **2016**, *421*, 57–65. [\[CrossRef\]](#)
- Gnanaprakasam, A.; Sivakumar, V.M.; Thirumarimurugan, M. Influencing Parameters in the Photocatalytic Degradation of Organic Effluent via Nanometal Oxide Catalyst: A Review. *Indian J. Mater. Sci.* **2015**, *2015*, 601827. [\[CrossRef\]](#)